Electrode Processes in Molten Carbonate Fuel Cells

Isaac Trachtenberg
Corporate Research & Engineering, Texas Instruments Incorporated, P. O. Box 5474, Dallas 22, Texas

Introduction

Many of the potential applications of fuel cells require operation on cheap, readily available fuels and air. These fuels in all probability will be hydrocarbons or impure fuel gases readily derived from hydrocarbons. Fuel cells employing molten carbonate electrolytes and operating above 500°C afford an early opportunity for rapid development of a system capable of satisfying these requirements. The material presented here is concerned with some of the more fundamental aspects of molten carbonate-magnesium oxide-matrix cells. The causes of electrode polarization are established and measured. Typical data for the effect of fuels on anode polarization are given. Based on the experimental observations, chemical and electrochemical reaction schemes are suggested. Theoretical voltage-fuel composition curves are illustrated and indicate that good utilization of fuel at reasonable voltages can be expected. Cells have actually operated on hydrocarbon fuels and air at acceptable power levels continuously over extended time intervals.

Fuel cells employing various eutectics of molten alkali carbonates as the electrolyte have been previously described.[1-4] Operating characteristics of magnesium oxide (MgO) matrix cells have also been reported.[5-7] These cells have been thermally cycled a number of times and in some instances attained more than 4000 hours of continuous operation at 600°C. Power densities greater than 100 watts/ft^2 at 0.7 volts have been obtained with pure hydrogen fuel and 4:1 air: CO_2 mixtures as the cathode gas feed. These results have led to the initiation of design and development work on molten-carbonate hydrocarbon fuel cell batteries and systems. However, discussion of these engineering studies is beyond the scope of this paper.

Experimental

All of the experimental work reported here was performed on cells identical to that shown in Fig. 1. This illustration shows the cathode chamber of the cell with the third idling electrode. This small electrode is used to monitor the performance of the individual anode and cathode in a working fuel cell. The large electrode (15.6 cm^2 or 1/60 ft^2) is the working cathode and is bonded to the MgO matrix. The matrix is impregnated with the binary $LiNaCO_3$ eutectic (m.p. ca. 500°C). Not shown is the anode bonded on the bottom side of the MgO matrix. The anode has the same geometrical configuration and area as the cathode. Cathodes for this study were pure silver; however, substrates of base metals containing catalyst are now being used successfully. The anode is made of either silver or base metal substrates containing a wide variety of inexpensive catalyst.

Electrical connections are made from the electrodes to the various insulated lead-throughs. The only electrical connection within the cell between the three electrodes is through the electrolyte contained in the MgO matrix. The lids are then welded on to make each chamber gas tight. The cell is placed vertically in a furnace and the necessary external gas and electrical connections are completed.

Current-voltage traces for the complete working cell and the individual electrodes were obtained with a Moseley Model 3S X-Y recorder. A transistor network is used to give a continuously variable, pure resistive, load for the cell. The current passed in this circuit is the X-input. The voltage between the non-working electrode and the particular working electrode to be studied, or the terminal voltage of the cell becomes the Y-input. In order to avoid polarization of the non-working electrode the Y-input or for that matter any voltage measuring device used with the non-working electrode must have a high input impedance. These current-voltage curves measure the total steady-state polarization of the individual electrodes and the complete cell under working conditions.

In order to establish the contributions of the various types of polarization, ohmic, activation, and concentration, to the total polarization, it is necessary to resort to a transient method. A single current interruption technique was used for this purpose. The three types of polarization of interest may be distinguished according to time intervals after removing the polarizing load. Ohmic polarization is removed immediately after current interruption for the present investigation in times less than a microsecond. Since removal of activation polarization requires the electrode potential to change, the time required for its decay is governed by the rate of charging of the electrical double layer or about 10^{-6} to 10^{-4} seconds. Polarization decay because of concentration effects requires times greater than 10^{-4} seconds since appreciable mass transport (either ions in the electrolyte or molecules in gas phase) must occur.

Figure 2 schematically shows the interruption circuit. The heart of this circuit is the mercury wetted Clare relay and its make before break operating feature. This latter feature permits triggering and use of the sweep delay circuits of the 545A oscilloscope. Voltage time curves are recorded from the oscilloscope from 10^{-6} to 1 second.[7]

Current-Voltage Curves for Operating Cell

The specific results presented are typical examples of the data obtained from a large number of experiments on many similar cells. Figure 3 is current-voltage curves for a cell operating at 600°C on pure H_2 fuel on the 25th day of operation. The cathode is supplied with a 4:1 mixture of air:CO_2. The curve V_T represents the terminal voltage of the operating cell. The open circuit voltage is 1.40 volts. V_A and V_C curves are the voltage of the anode and cathode, respectively, versus the non-working electrode. The values of R_A and R_C, the ohmic resistances as determined by current interruption, were measured at several pre-interruption currents and found to be constant. Correction for the ohmic polarization is made and the curves $V_A + IR_A$ and $V_C - IR_C$ are the current-voltage curves due to concentration polarization. It is interesting to note that $R_A + R_C < R_T$. This difference is assumed to be the bulk electrolyte resistance, R_E. In addition to the ohmic resistance at the electrode-electrolyte-matrix interface, R_A and R_C contain the resistance of the individual electrode leads to the terminals just outside of the furnace. For the particular case of cell 117R at 600°C, R_A, R_C, and R_T are 0.075, 0.10, and 0.21 ohms, respectively; the lead resistance of the individual electrodes is about 0.025 ohms. R_E is calculated to be .035 ohms. The calculated resistance based on electrolyte conductivity, electrode size, and separation is .011 ohms. These calculations imply a factor due to porosity and tortuosity of the MgO disc of about 3.

The V_T curve indicates a power density equivalent to 60 w/ft^2 at 0.7 volts. If all ohmic factors with the exception of the bulk electrolyte resistance, R_E, could be removed, this cell would produce an equivalent of 120 watts/ft^2 at 0.7 volts.

Several features concerning the polarization of the individual electrodes should be pointed out. Limiting currents are not being approached even at current densities of 200 amps/ft^2. Ohmic polarization is a more important factor at the cathode, where oxide films may be formed. Concentration polarization is greater at the anode, since products must back diffuse.

Figure 4 shows additional current-voltage curves for cell 117R. In order to obtain these data, 200 cc/min of CO_2 were added to the original H_2 fuel supply. This fuel represents a reformed hydrocarbon. The cathode conditions were unchanged and the same polarization curves were obtained for it as in Fig. 3. The effect of additional flow rate by itself is negligible (H_2 rate was raised to 700 cc/min with no measurable change in the current-voltage curve). The effect of adding CO_2 was observed immediately even at open circuit. Considerable amounts of water were obtained in the fuel effluent. The values of R_A, R_C and R_T were not altered by the change in fuel composition. However, the open circuit voltage is markedly reduced and can be attributed to the introduction of CO_2 and the formation of H_2O from the water-gas shift equilibrium. These substances are products from the overall anode process.

The terminal power output is equivalent to 42 watts/ft^2 at 0.7 volts and if all ohmic factors excluding bulk electrolyte resistance were eliminated, an equivalent power of about 84 watts/ft^2 at 0.7 volts could be obtained. It should be noted in comparing figures 4 and 3 that the concentration polarization, 0.18 volts, at an equivalent of 100 amps/ft^2 for reformed hydrocarbon fuel is considerably lower than that of the pure H_2 fuel, 0.35 volts, at the same current density. However, the open circuit voltage and the operating voltage is lower for the reformed fuel, 1.06 volts open circuit, compared to 1.40 volts open circuit, for the pure H_2 fuel.

What has been referred to as concentration polarization until now is really total polarization minus ohmic polarization. From data such as these and current interruption studies, no activation polarization or evidence of any could be detected. As might be expected, the system is subject to less concentration polarization as product concentration of the incoming fuel increases.

Current Interruption Studies

As previously mentioned the various types, ohmic, activation, and concentration polarization may be distinguished and measured by voltage decay as a function of time after interruption of a steady state current. A previous publication[7] was concerned only with pure H_2 fuel in this system. Comparison of hydrogen with simulated reformed hydrocarbon fuels is presented here.

Figure 5 illustrates anode current-voltage curves corrected for ohmic polarization. Open circuit voltage decreases with decreasing flow rate and increasing product (CO_2 and H_2O) concentration. However, polarization at any given current density decreases with increasing product concentration of the incoming fuel. The lower open circuit voltage of curve B compared to curve A is related to the amount of CO_2 continuously escaping from the electrolyte and the relative concentration of CO_2, H_2O and H_2 (see proposed reaction scheme).

Current interruption experiments were completed with the fuels indicated in Fig. 5. All measurements were made at a pre-interruption current equivalent to a current density of 60 amps/ft^2. Figure 6 illustrates the voltage-time curves for the two high fuel flow rates. The two straight lines are characteristic of this type measurement. The steady state polarization is represented by the symbols through the ordinate. The initial drop is the same for all fuels and flows studied. Data in the 10^{-6} range are somewhat distorted by the ring-back voltage which develops when the current drops instantly to zero. The horizontal line in the 10^{-5} to 10^{-4} second range indicates no measurable activation polarization. The polarization decay in times greater than 10^{-4} are attributed to concentration effects. The two curves are almost parallel. At the high flow rates used, any effect of flow rate has been removed. Since polarization for the H_2-CO_2 fuel is less than that for pure H_2, the H_2-CO_2 open circuit voltage is attained more rapidly.

Figure 7 illustrates the voltage time curves for the lower flow rates of Fig. 5. The same characteristic features are observed here as in Fig. 6. The ohmic polarization is constant and there is no measurable activation polarization. However, there is an effect of flow rate. The total flow of 360 cc/min for H_2-CO_2 case increases the rate of decay of concentration polarization over that observed for pure H_2 at 160 cc/min.

The effect of flow rate on anode polarization curves was studied in another series of experiments. In Fig. 8 anode polarization curves corrected for ohmic polarization at various fuels and flow rates are presented. Curve I illustrated that cells operating on reformed hydrocarbons at high flow rates perform better than on pure H_2 even though the open circuit voltage is higher for the pure fuel. The introduction of an inert gas to aid sweep, curve III, leads to high open circuit voltage but polarizes much more rapidly (compare curves II and III) when placed under load.

All of those data relating to flow rates indicate that the benefits of high open circuit voltage obtained by high flows of pure hydrogen or hydrogen diluted with inert gases is lost when significant quantities of the fuel are consumed. The effect of the high flow rates of gases is to reduce the concentration of non-electrochemically produced CO_2 and H_2O. When the electrochemical processes are functioning, this effectiveness of gas sweeping is greatly reduced.

Interruption studies were made on cathodes. Figure 9 is a typical voltage-time plot for a cathode operating on a 4:1 misture of air:CO_2. The curves are very similar to those obtained for anodes. Cathodes exhibit higher ohmic polarization than anodes and less concentration polarization. Cathodes are not as sensitive to gas flows. Since concentration polarization is small, electrode steady state is rapidly attained.

Ohmic Polarization and Electrolyte Resistance

Ohmic resistance at the individual electrodes is calculated from the initial (10^{-6} second) voltage decay and the pre-interruption current. The values determined include lead resistance (.025 ohms). Bulk electrolyte resistance is determined by subtracting the sum of the anode and cathode resistance from the total cell resistance.

The temperature coefficients of the various resistances were measured. The coefficient of anode was nearly identical with that of bulk electrolyte, while the co-

efficient of the cathode was much higher (resistance decreased more than would be predicted on the basis of changes in electrolyte conductivity alone).

The relatively high ohmic polarization, the consequence of ohmic resistance, at the anode may be attributed to electrolyte restriction at the electrode-matrix interface. It is very unlikely that all pores of the electrode match the pores in the matrix. In fact, there is a great deal of masking. This masking greatly reduces the thickness and number of electrolyte paths between the active electrode sites and the bulk electrolyte and increases the ohmic resistance. Since the temperature coefficient of the ohmic resistance at the anode is the same as the bulk electrolyte, it is reasonable to assume that all of the ohmic polarization at this electrode is due to the electrolyte. Its relatively large value is directly attributable to the degree of electrolyte restriction.

At the cathode a similar situation exists. However, there is an additional contribution to the ohmic resistance which has a larger temperature coefficient. Although silver oxide is thermally unstable at 600°C there is a finite amount present on the electrodes. This oxide layer introduces some additional ohmic resistance. As the temperature is increased the amount of oxide is reduced and the ohmic polarization decreases.

Reaction Scheme for Overall Electrode Processes

The foregoing experiments and results suggest that all reaction kinetics are very fast and equilibriums are established. The observed polarization is attributed to ohmic resistances and mass transport limitations. At the anode the same types of polarizations exist for pure H_2 fuel as for a variety of H_2-CO_2 fuels which represent reformed and partially consumed reformed hydrocarbon fuels.

Two chemical reactions are assumed to always be in equilibrium:

1) $H_2 + CO_2 \rightleftharpoons H_2O + CO$

2) $CO_3^{=} \rightleftharpoons CO_2 + O^{=}$ 8.9

The oxide ion is the active potential determining species present in the electrolyte. The electron-transfer reaction becomes

3) $M + O^{=} \rightleftharpoons MO + 2e^{-}$

where M represents the active metal catalysts. Fuel is consumed in the chemical reduction of the metal oxide by H_2

4) $MO + H_2 \rightleftharpoons M + H_2O$,

thus regenerating the active metal catalysts. At 600°C and higher, this latter reaction proceeds rapidly and is always in equilibrium. The equilibrium being shifted very far toward metal-water.

On the basis of this model the anode potential may be represented as

5) $$E_A = E_A^o - \frac{2.3\,RT}{nF} \log \frac{\left[a_{H_2O}\right]\left[a_{CO_2}\right]}{\left[a_{H_2}\right]}$$

where a_i represents the activity of the various reactants and products. The various activities are represented in terms of a contribution from electrochemical and chemical reaction. For example

6) $a_{H_2O} = \Theta_{H_2O}(x + y)$

where Θ_{H_2O} is a proportionality constant, x is partial pressure of water obtained from electrochemical conversion and y is the partial pressure of water obtained by shift conversion.

Figure 10 illustrates anode potential curves obtained assuming Θ_{H_2O}, Θ_{H_2O} and Θ_{CO_2} all equal to 1. The initial fuel is pure H_2. The potential is plotted as a function of the H_2 electrochemically consumed. The potential scale is meant to be a relative scale since E_A^o was assumed to be standard potential for the reaction,

7) $H_2 + 1/2O_2 \rightleftharpoons H_2O$,

at the appropriate temperature. The dashed line is the same plot neglecting the shift reaction.

In Fig. 11 the value of Θ_{H_2O} was varied and a family of curves with the same potential variation with H_2 consumption was obtained. In all of these curves the cathode is invariant. Θ_{H_2O} represents a weighting factor for surface coverage. Since CO_2 pressure effects the potential by establishing the equilibrium concentration of $O^=$, its weighting factor is always unit. However, there is competition for metal sites between H_2 and H_2O. The weighting factor indicates the ratio of H_2O-coverage to H_2-coverage when the partial pressure of the two components is equal. As figure 11 indicates, Θ_{H_2O} merely changes the absolute anode potential for a given E_A^o. This value of Θ_{H_2O} for an electrode will depend upon the metal catalyst.

Figure 12 illustrates the effect of starting with fuels obtained from various hydrocarbon treating processes. Curves A and B represent steam reforming with limited purification of the raw reformate. Curve C represents completely reformed and shifted natural gas. Curve D represents partial oxidation of hydrocarbons of the class C_nH_{2n}. Curve E is a 80% consumed fuel in which all the water is removed. At low consumption there is appreciable benefit for initially supplying a pure H_2. However, at more than 50% electrochemical consumption of the starting fuel there is very little advantage for the use of pure H_2 and various partially oxidized hydrocarbons may be used with equal effectiveness.

The proposed reaction scheme for cathodes[7] is similar to anodes. The first step in the scheme is the adsorption of O_2.

8) $O_2 + nAg \rightleftharpoons 2Ag_{n/2}O$.

This oxide formation is responsible additional ohmic resistance observed at the cathode. The electrochemical reaction is

9) $2Ag_{n/2}O + 4e^- \rightleftharpoons nAg + 2O^=$

and finally the equilibrium between CO_2 and $O^=$,

10) $2CO_2 + 2O^= \rightleftharpoons 2CO_3^=$,

is established at the cathode. The potential of the cathode may be written as

11) $$E_C = E_C^o - \frac{2.3\,RT}{nF} \log \left[\frac{1}{(a_{O_2})(a_{CO_2})^2} \right]$$

where a_{O_2} and a_{CO_2} are the activities (partial pressures) of oxygen and CO_2.

According to equation 11 the substitution of O_2 for air should increase the overall cell voltage about 30 millivolts. This predicted result has been verified experimentally.

Conclusion

Fuel cells employing molten-carbonate electrolytes can be operated successfully on air and a wide variety of fuels readily derived from hydrocarbons. At current densities up to 200 amps/ft^2 there is no kinetic limitation other than mass transport.

When hydrocarbon-derived fuels are initially supplied to the anode, open circuit voltage is lower than when pure H_2 is supplied. However, under appreciable load, anode polarization on impure fuel is much lower. Cathodes perform well on mixtures of air and CO_2.

Although all of the electrodes investigated showed no activation polarization, electrode potential under operating conditions is dependent on the product-reactant adsorption equilibrium of the particular catalyst-electrode.

Acknowledgements

In part the work reported here received financial support from the United States Army Engineers Research and Development Laboratories, Fort Belvoir, Virginia

References

1. G. H. J. Broers, "High Temperature Galvanic Fuel Cells" Thesis, University of Amsterdam (1958).
2. G. H. J. Broers and J. A. A. Ketellaar in "Fuel Cells", G. J. Young, Editor, pp 78-93, Reinhold Publishing Co. (1960).
   H. H. Chambers and A. D. S. Tantrum, ibid., pp 94-100.
3. M. L. Kronenberg, J. Electrochem. Soc. 109, 753 (1962).
4. Y. L. Sandler, ibid 109, 1115 (1962).
5. C. G. Peattie, B. H. Barbee, K. W. Kreiselmaier, S. G. Parker, I. Trachtenberg, and A. H. White, "Performance Data for Molten-Electrolyte Fuel Cells Operating on Several Fuels", Conference Proceedings 1962, Pacific Energy Conversion Conference, San Francisco, Calif., Aug. 12-16, 1962.
6. C. G. Peattie, I. Trachtenberg, B. H. Barbee, K. W. Kreiselmaier, S. G. Parker and A. H. White, "Factors Involved in the Use of a High Temperature Fuel Cell as a Space Power Source", Vol. II, Progress in Astronautics and Rocketry "Power Systems for Space Flight" in press (1963).
7. I. Trachtenberg, J. Electrochem. Soc., in press (1963).
8. H. Flood, T. Forland, and K. Motzfeldt, Acta. Chem. Scand. 6, 257, (1952).
9. S. Djordjevic and G. J. Hills, Trans. Faraday Soc. 56, 269 (1960).

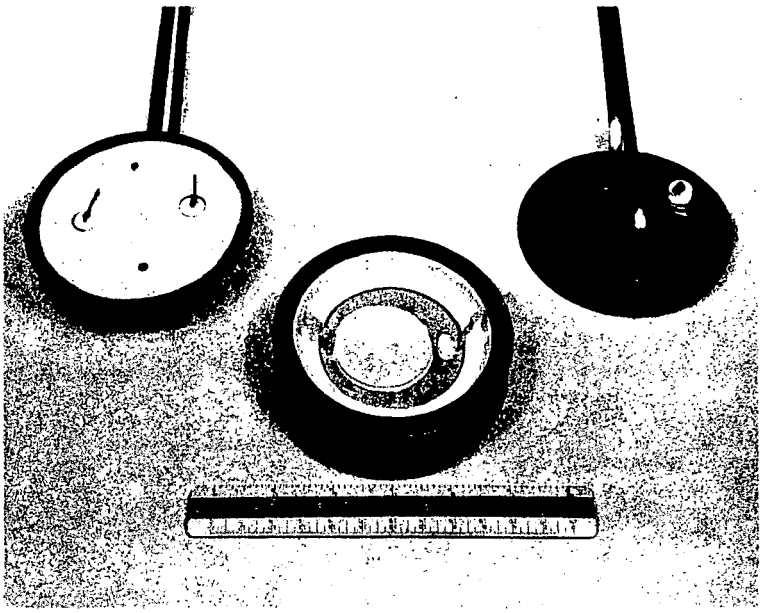

Fig. 1 Cathode chamber of a working fuel cell showing third idling electrode

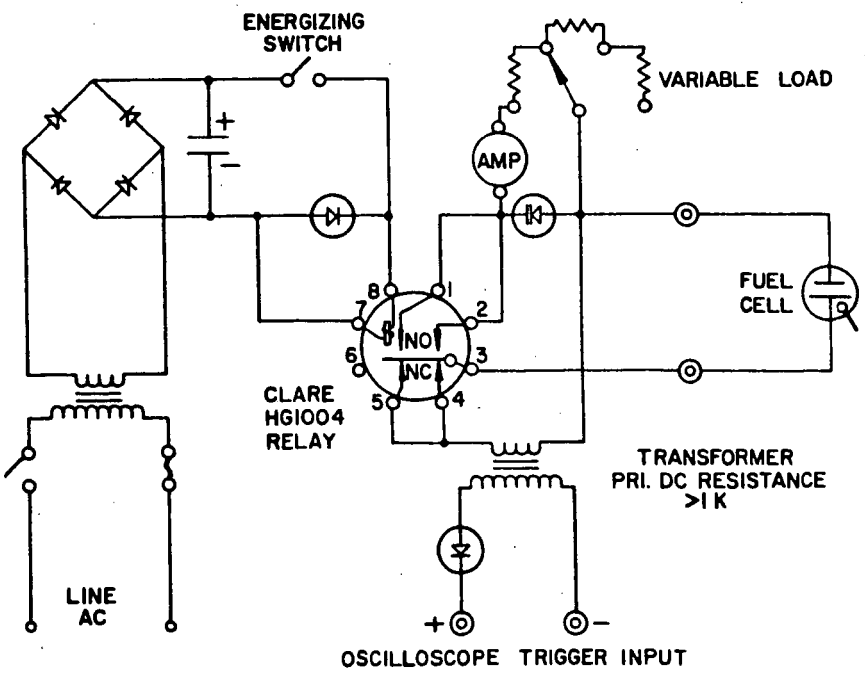

Circuit used to obtain voltage−time curve < 1 sec.

Fig. 2 Interrupter circuit

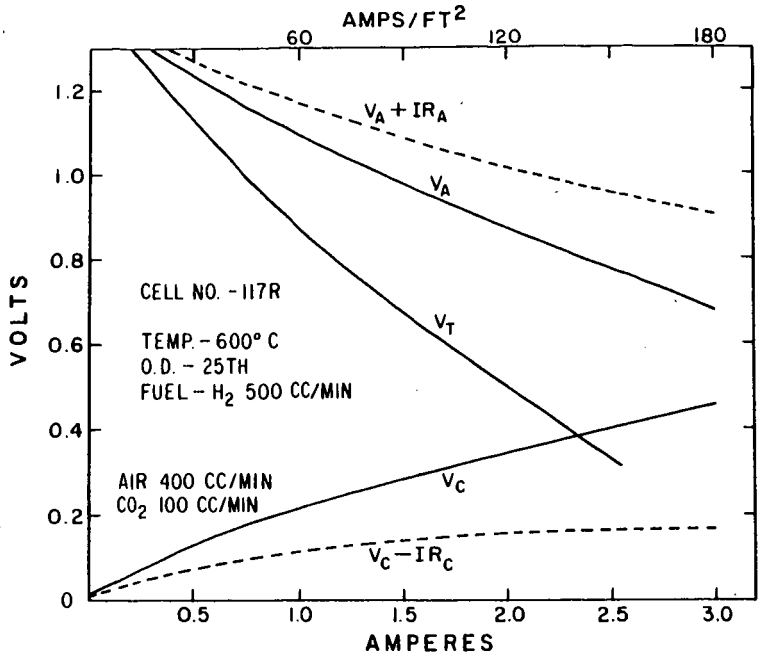

Fig. 3 Typical polarization curves for a cell and individual electrodes operating on H_2 and air-CO_2

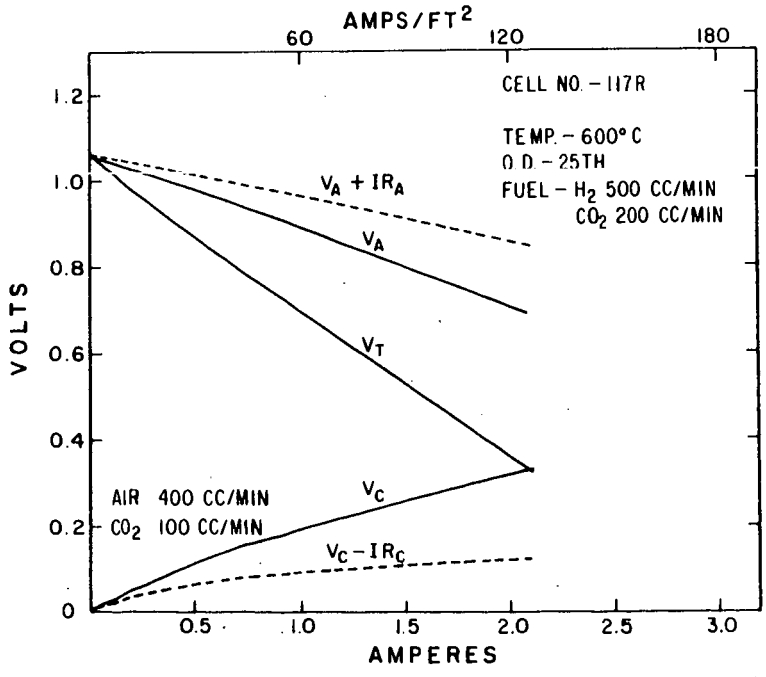

Fig. 4 Typical polarization curves for a cell and individual electrodes operating on a simulated reformed hydrocarbon and air-CO_2

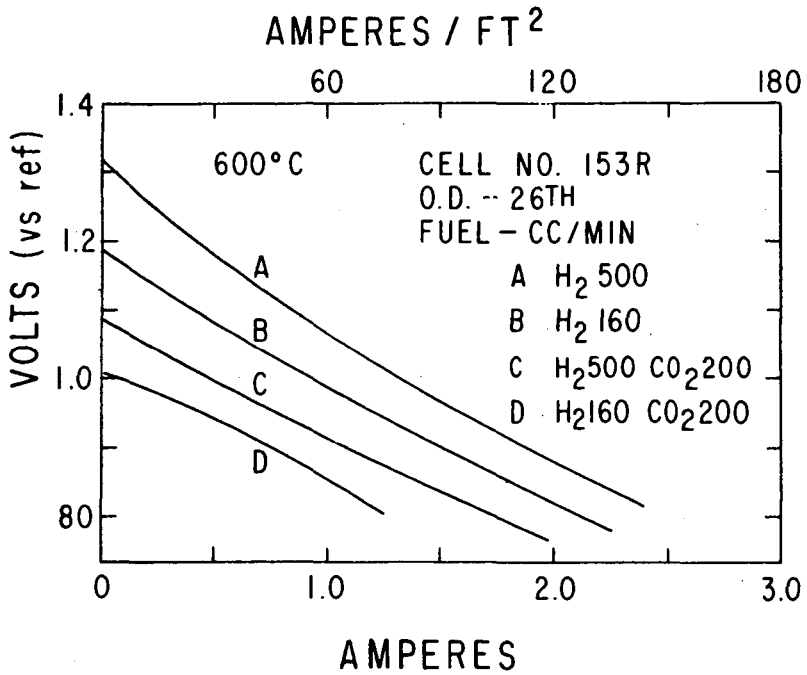

Fig. 5 Anode polarization curves corrected for ohmic polarization. Data obtained from operating cell.

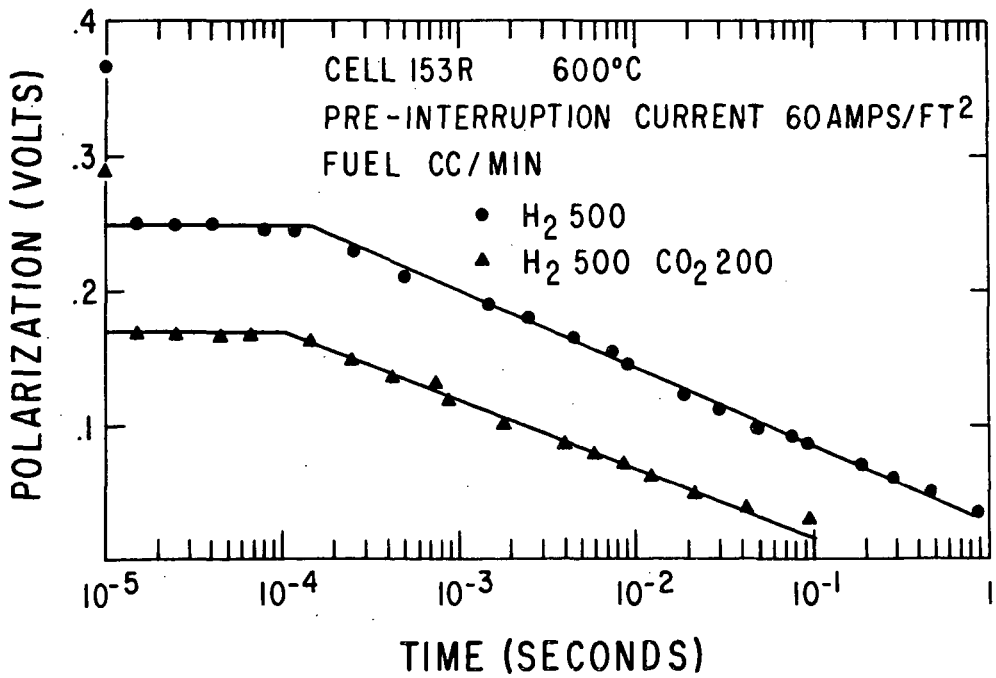

Fig. 6 Anode polarization-time curves after interruption of 1.0 amp.

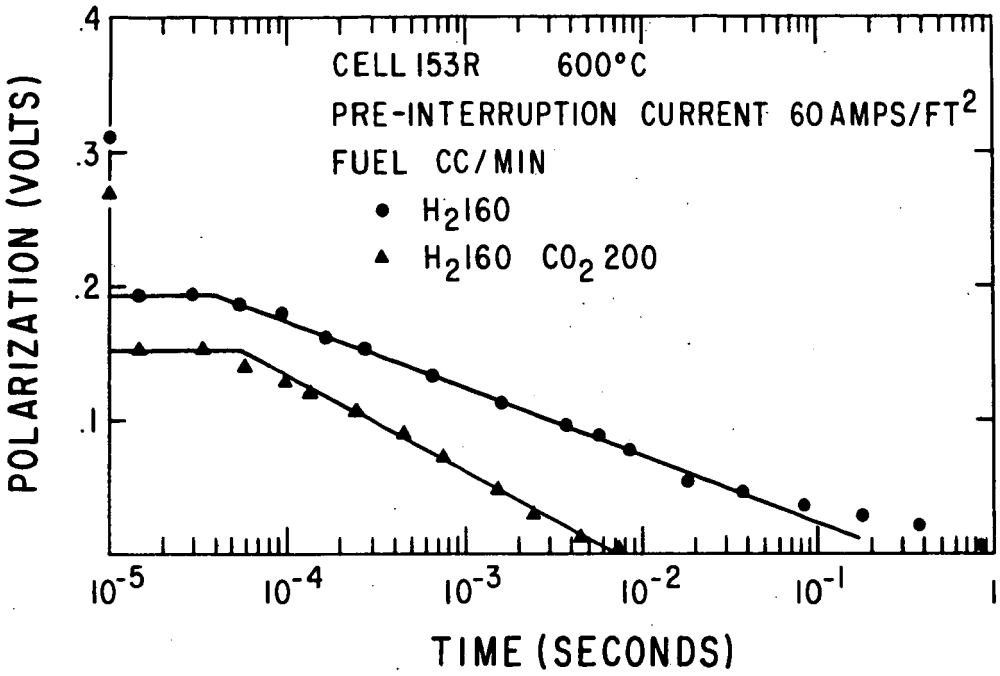

Fig. 7 Anode polarization-time curves after interruption of 1.0 amp.

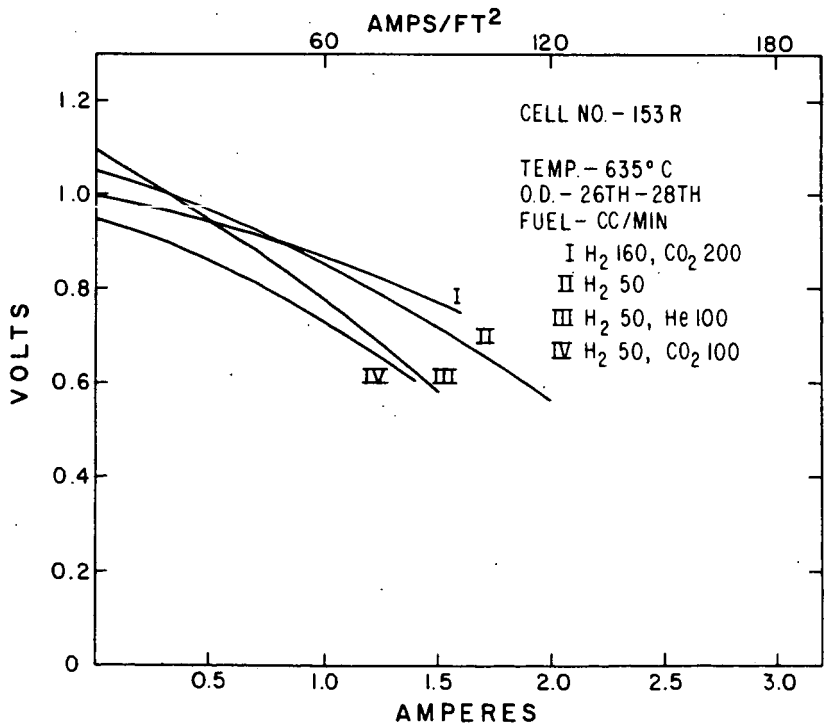

Fig. 8 Anode polarization curves corrected for ohmic polarization. Data obtained from operating cell varying fuel composition and flow rate.

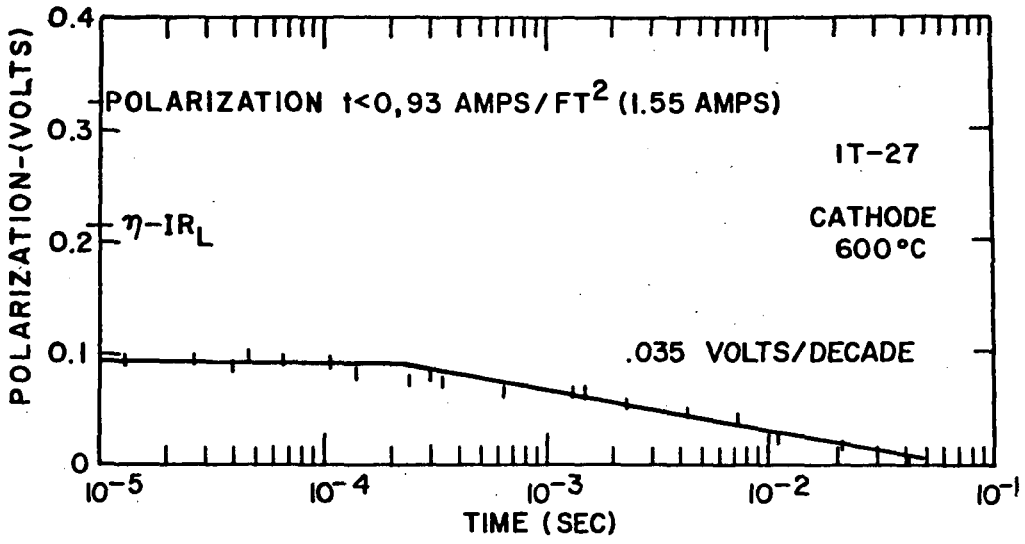

Fig. 9 Cathode polarization-time curve for typical cathode after interruption of 1.55 amps.

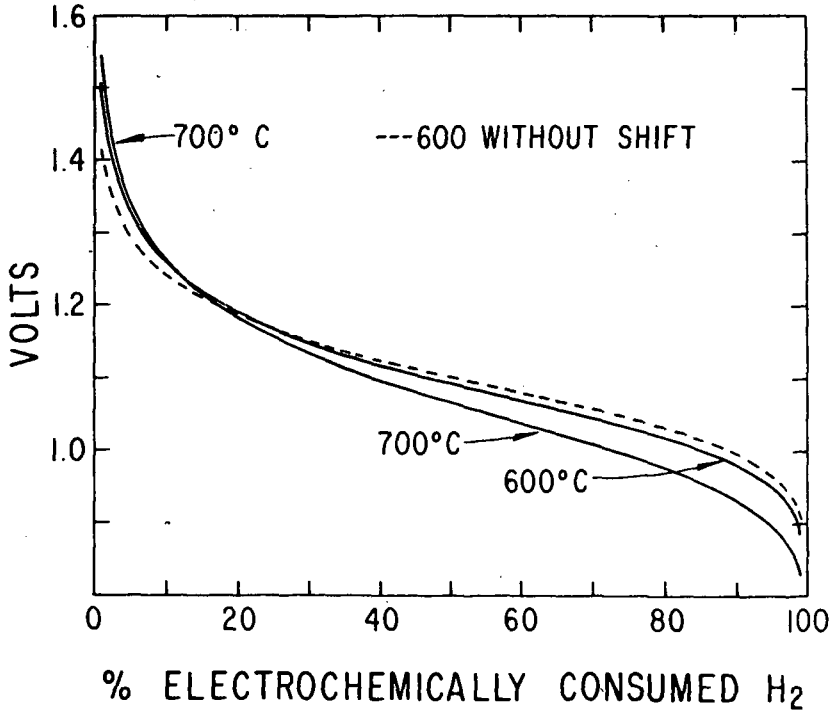

Fig. 10 Calculated potential-fuel consumption curves for anodes

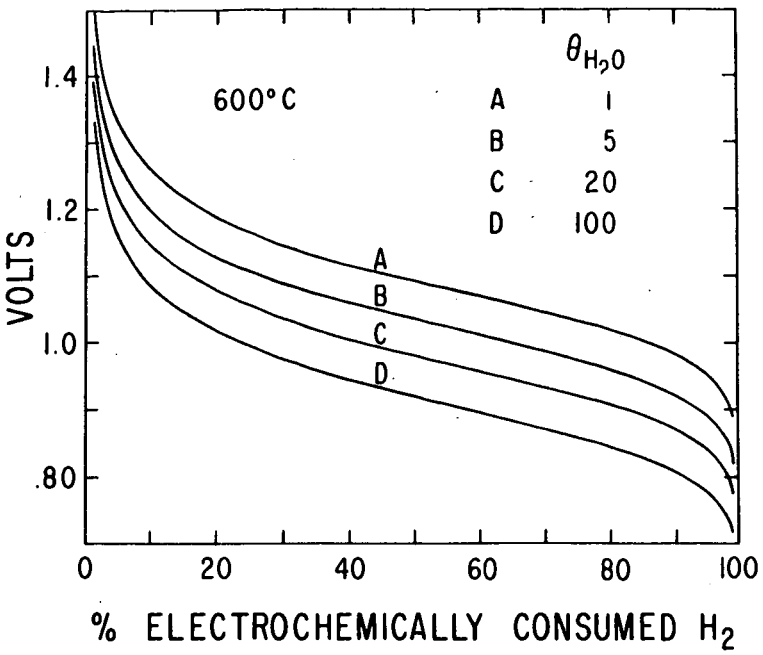

Fig. 11. Calculated potential-fuel composition curves for anodes assuming various ratio of H_2O:H_2 adsorption

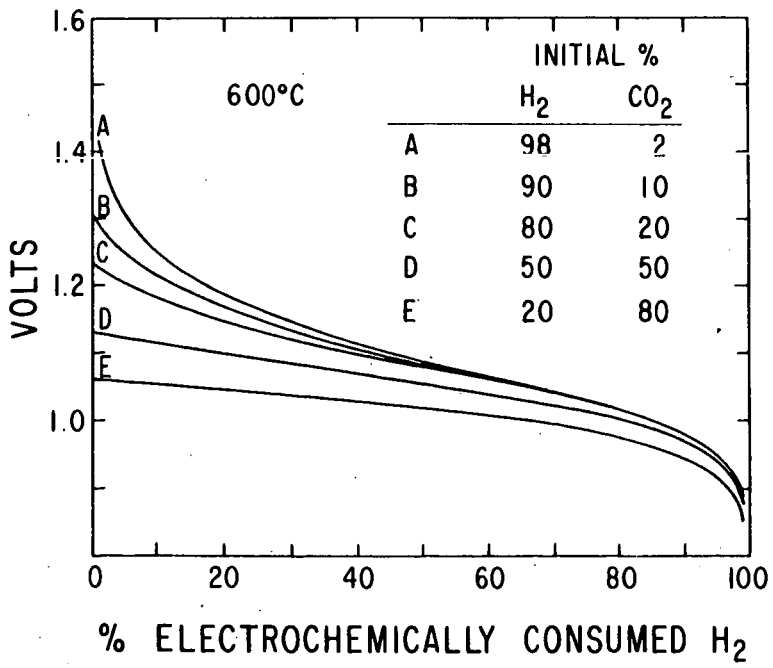

Fig. 12 Calculated potential-fuel composition curves for anodes varying composition of starting fuel